

See discussions, stats, and author profiles for this publication at: <https://www.researchgate.net/publication/229733559>

Euler deconvolution of the analytic signal and its application to magnetic interpretation

Article in Geophysical Prospecting · April 2004

DOI: 10.1111/j.1365-2478.2004.00408.x

CITATIONS

99

READS

1,298

2 authors:



Pierre Keating

Consultant

106 PUBLICATIONS 1,210 CITATIONS

[SEE PROFILE](#)



Mark Pilkington

Natural Resources Canada

136 PUBLICATIONS 4,935 CITATIONS

[SEE PROFILE](#)

Some of the authors of this publication are also working on these related projects:



Silurian-Devonian Gaspé Belt in eastern Canada: evolution and resource potential [View project](#)

Euler deconvolution of the analytic signal and its application to magnetic interpretation

P. Keating* and M. Pilkington

Geological Survey of Canada, Continental Geoscience Division, 615 Booth Street, Ottawa, Ontario K1A 0E9, Canada

Received October 2001, revision accepted December 2003

ABSTRACT

Euler deconvolution and the analytic signal are both used for semi-automatic interpretation of magnetic data. They are used mostly to delineate contacts and obtain rapid source depth estimates. For Euler deconvolution, the quality of the depth estimation depends mainly on the choice of the proper structural index, which is a function of the geometry of the causative bodies. Euler deconvolution applies only to functions that are homogeneous. This is the case for the magnetic field due to contacts, thin dikes and poles. Fortunately, many complex geological structures can be approximated by these simple geometries. In practice, the Euler equation is also solved for a background regional field. For the analytic signal, the model used is generally a contact, although other models, such as a thin dike, can be considered. It can be shown that if a function is homogeneous, its analytic signal is also homogeneous. Deconvolution of the analytic signal is then equivalent to Euler deconvolution of the magnetic field with a background field. However, computation of the analytic signal effectively removes the background field from the data. Consequently, it is possible to solve for both the source location and structural index. Once these parameters are determined, the local dip and the susceptibility contrast can be determined from relationships between the analytic signal and the orthogonal gradients of the magnetic field. The major advantage of this technique is that it allows the automatic identification of the type of source. Implementation of this approach is demonstrated for recent high-resolution survey data from an Archean granite-greenstone terrane in northern Ontario, Canada.

INTRODUCTION

Automated interpretation techniques are commonly used to interpret large data volumes efficiently. Euler deconvolution uses the magnetic field and its three orthogonal gradients (two horizontal and one vertical) to compute anomaly source locations. The field is sampled on a rectangular grid interpolated from the original data distribution. Usually, gradients are computed from the interpolated field, but measured gradients can be used when available. Thompson (1982) included a background field in the Euler equation to minimize the effect of neighbouring anomalies and to remove any bias from the observed field. Estimation of the correct structural index

is crucial for the successful application of the method (Reid 1995). This is achieved either based on experience, or by trial and error, or by using an index that produces the best clustering of solutions (Reid *et al.* 1990). Horizontal source locations are usually well determined by Euler deconvolution, so that an incorrect choice of structural index leads to errors in the estimated source depths (Ravat 1996; Barbosa, Silva and Medeiros 1999).

The three-dimensional (3D) analytic signal is calculated from the three orthogonal gradients of the magnetic field (Roest, Verhoef and Pilkington 1992). The signal reaches a maximum directly above magnetization contrasts and is independent of the ambient magnetic field and source magnetization directions. Assuming that anomalies are caused by vertical contacts, the analytic signal can be used to estimate depths to

*E-mail: pkeating@nrcan.gc.ca

magnetic sources. Thurston and Smith (1997) estimated edge locations, depths, dips and susceptibility contrasts from magnetic anomalies using the complex analytic signal. Although the method uses gridded data, it is really a 2D method using profiles extracted from the grid using a sophisticated algorithm that estimates anomaly strikes. The sloping contact and the thin dike are the basic models. The method has been extended to horizontal cylinders and can also determine the most appropriate model (Smith *et al.* 1998). However, efficient and practical implementation of the method is difficult. Here, we propose using Euler deconvolution of the analytic signal to estimate magnetic source location and structural index. Dip and susceptibility contrast are later evaluated from relationships between the analytic signal and the first vertical derivative of the magnetic field. This technique is easier to implement than the Thurston and Smith (1997) technique for gridded data.

THEORY

Euler's homogeneity equation, when taking into account a base level for the background field, can be written as (Reid *et al.* 1990)

$$(x - x_0) dT/dx + (y - y_0) dT/dy + (z - z_0) dT/dz = N(B - T), \quad (1)$$

where T denotes the observed magnetic field at (x, y, z) , (x_0, y_0, z_0) is the source anomaly location (note that z_0 is the depth below the magnetic sensor), B denotes the base level of the observed field, and N denotes the structural index.

Since a regular grid is used, the equations can be solved over a small window. A 3×3 window results in an overdetermined system of equations from which the four unknowns (x_0, y_0, z_0, B) and their estimated errors are obtained. These estimated errors are often normalized by the calculated depth and expressed as percentages (Thompson 1982). The technique is implemented by solving the system of equations from a moving window. For large grids this can result in many thousands of solutions. Good solutions are those that group together well and have a small relative error. Barbosa *et al.* (1999) carried out an extensive stability analysis of Euler's equation and proposed a technique to select the correct index. This study was restricted to the 2D case but could probably be extended to 3D sources. They proposed that the correct index is the one that minimizes the correlation between the observed anomaly and the base level over a series of adjacent moving windows. This clearly demonstrates the importance of the base level in the solution of Euler's equation. It is evident from (1) that if

the base level were known, it would be possible to calculate directly the structural index in addition to the source location.

Marson and Klingele (1993) have shown the advantages of using the vertical gradient of gravity for Euler deconvolution of gravity data. They solved Euler's equation in a moving window over only areas that contain the maxima of the amplitude of the analytic signal or of the horizontal derivative. Again, the choice of the optimum structural index is based on the standard error of the solutions and their clustering. It should be noted that solving Euler's equation for the vertical gravity gradient anomaly without any base level is equivalent to solving Euler's equation for the gravity anomaly when a constant base level is included. Although the solution of Euler's equation for the vertical gradient of the magnetic field allows the determination of the structural index, it is better to work with the analytic signal as it also allows us to determine the dip, depth and susceptibility contrast of the causative body.

Huang *et al.* (1995) have shown that if a function is homogeneous of degree N , then its analytic signal is homogeneous of degree $N + 1$. This is easily verified for simple models such as a contact, a thin dike and a monopole. Euler's equation then becomes

$$(x - x_0) dA/dx + (y - y_0) dA/dy + (z - z_0) dA/dz = -NA, \quad (2)$$

where A denotes the analytic signal of the magnetic field.

The analytic signal can therefore be processed in the same way as total field data are processed in standard Euler deconvolution. The structural indices are simply one greater when using analytic signal data (and its three orthogonal derivatives). The advantage is that taking derivatives to calculate the analytic signal effectively removes the (unknown) background or base level field B in (1). Consequently, instead of specifying N and solving (1) for x_0, y_0, z_0 and B , we can now ignore B and solve for x_0, y_0, z_0 and N directly. This removes the need for computing Euler solutions for a number of different values of N and then determining N for a given structure based on the clustering of solutions.

In order to determine source parameters other than location, we require quantities related to the analytic signal and the vertical magnetic field gradient. The analytic signal over a magnetic contact located at x_0 and depth z_0 is (Nabighian 1972)

$$A(x, z) = \alpha \frac{1}{((x - x_0)^2 + (z - z_0)^2)^{1/2}}. \quad (3)$$

For a 2D magnetic sheet, it is (MacLeod, Jones and Fan Dai 1993)

$$A(x, z) = \alpha \frac{1}{((x - x_0)^2 + (z - z_0)^2)}, \quad (4)$$

where α is given below.

Over a horizontal cylinder the analytic signal is given by (MacLeod *et al.* 1993)

$$A(x, z) = \alpha \frac{2}{((x - x_0)^2 + (z - z_0)^2)^{3/2}}. \quad (5)$$

Therefore, structural indices for these models will be 1 for a contact, 2 for a sheet and 3 for a horizontal cylinder, which is one more than the structural indices for the corresponding total magnetic field anomalies. A magnetic monopole, which can be used to represent a vertical pipe (Reid *et al.* 1990), also has an index of 3 for its analytic signal. Different sources can have the same structural index, although they are easy to distinguish in plan view. Once the source location (x_0, z_0) and the structural index N are known it is easy to determine α and calculate the susceptibility. In the case of a sheet, it is only possible to determine the susceptibility-thickness product, whereas in the case of the horizontal cylinder, it is possible to determine the product of its cross-sectional area and the susceptibility.

At its maximum, the analytic signal has values:

$$A(0) = \alpha/z_0 \quad \text{for a contact}, \quad (6)$$

$$A(0) = \alpha/z_0^2 \quad \text{for a sheet}, \quad (7)$$

$$A(0) = 2\alpha/z_0^3 \quad \text{for the horizontal cylinder}. \quad (8)$$

Dip can be calculated using the method proposed by Nabighian (1972) who derived a relationship between the value of the horizontal gradient over the edge of a contact, its dip and susceptibility. Dip is obviously irrelevant for the horizontal cylinder. Here, to avoid sign ambiguity when working with gridded data, we prefer to use the vertical gradient V and have for a contact,

$$V(0) = \alpha \sin \phi / z_0, \quad (9)$$

where $V(0)$ is the vertical gradient at x_0 , $\alpha = 2kFc \sin d$ for a contact, $\alpha = 2kFcw$ for a sheet, z_0 is the depth of the source, $\phi = 2I - d - 90^\circ$ for a contact, $\phi = 2I - d$ for a sheet, k is the susceptibility contrast, F is the earth's magnetic field, w is the sheet thickness, $\tan I = \tan i/\cos A$, i is the inclination of the earth's magnetic field, A is the angle between magnetic north and the positive x -axis, $c = 1 - \cos^2 i \sin^2 A$, and d is the dip.

A similar relationship can be derived for the magnetic anomaly of a sheet or thin dike. In that case, we have

$$V(0) = \alpha \sin \phi / z_0^2 \quad (10)$$

From (5) and (8) it follows that for a contact we have the following relationship:

$$\sin \phi = V(0)/A(0). \quad (11)$$

An identical result is obtained for a sheet from (7) and (9). Determination of the structural index N allows us to estimate the dip d from ϕ . Interestingly, ϕ , the combined magnetic angle or effective dip angle, is independent of the structural index.

From (3)–(5) we have the following general relationship over the source ($x = x_0$):

$$A(0) = \alpha/z_0^N, \quad (12)$$

where α depends on source type (contact, sheet, etc.) and is independent of the depth z . Differentiating (12) with respect to depth gives

$$z_0 = N \frac{A(0)}{dA(0)/dz}. \quad (13)$$

Thus, if the structural index is known, it is possible to estimate the depth to sources from the ratio of the analytic signal to its vertical derivative. Source locations coincide with the maxima of both of these functions.

PROPOSED METHODOLOGY

In summary, the methodology we propose is to compute the structural index and source location by Euler deconvolution of the analytic signal and then determine the dip and the susceptibility contrast from the relationships involving the vertical derivative of the magnetic field (9) and the analytic signal (12). The technique can be used on both profile and gridded data as is the case for standard Euler deconvolution. The technique is implemented in a moving window fashion. As the window passes over the data, solutions naturally group in specific areas. For perfect data, all solutions are concentrated close to the true depth and location. In practice, for profile data, it is easy to compute solutions for a series of increasing window lengths or increasing number of data points. The best solutions can be selected on the basis of their relative errors. Reid *et al.* (1990) suggested using the relative error of the calculated depth; here, we also use the relative error of the calculated structural index.

SYNTHETIC DATA RESULTS

The method has been tested on profile and gridded data. For profile data, theoretical anomalies due to a contact and a dipping sheet were calculated for a depth of 100 m at a sampling interval of 10 m, i.e. about the sampling interval of high-resolution magnetic surveys. Field inclination in the plane of the profile was 75°. The vertical derivative used to compute the analytic signal was calculated in the frequency domain and the horizontal derivative was calculated in the space domain using finite differences. Calculated depths and analytic signal indices are accurate to better than 2%, and dips are within 3° of the true dip.

For gridded data, theoretical anomalies due to a sheet (Fig. 1) and a large vertical cylinder (Fig. 2) were used. In

both cases the magnetic field inclination was 75°N and the declination was 15°W. For the dipping sheet, the average calculated structural index is 1.996. For the large cylinder it is 1.018. The theoretical analytic signal structural index of the thin sheet is 2. For a contact, it is 1. It is also 1 for the large vertical cylinder since, locally, the side of the cylinder can be approximated by a contact if the local curvature of the cylinder is not too large. In both of the above cases, the depth was 100 m, the grid interval was 10 m and the size of the window used for the deconvolution was 10 grid intervals. The vertical cylinder has a radius of 1000 m. Histograms of the calculated depths and analytic signal structural index are shown in Figs 1 and 2. It can be seen that results for the thin dike are better than those for the vertical cylinder. Solution dispersion is larger for the cylinder than the sheet, due mostly to the

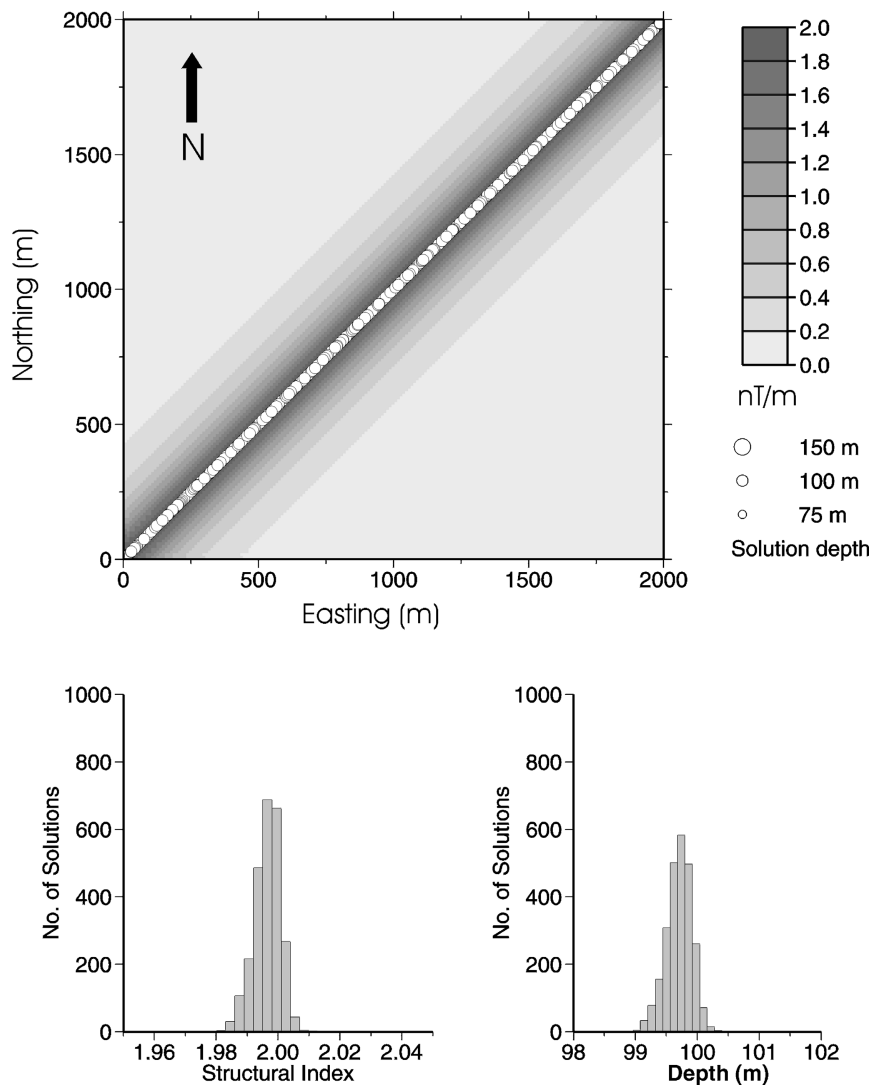
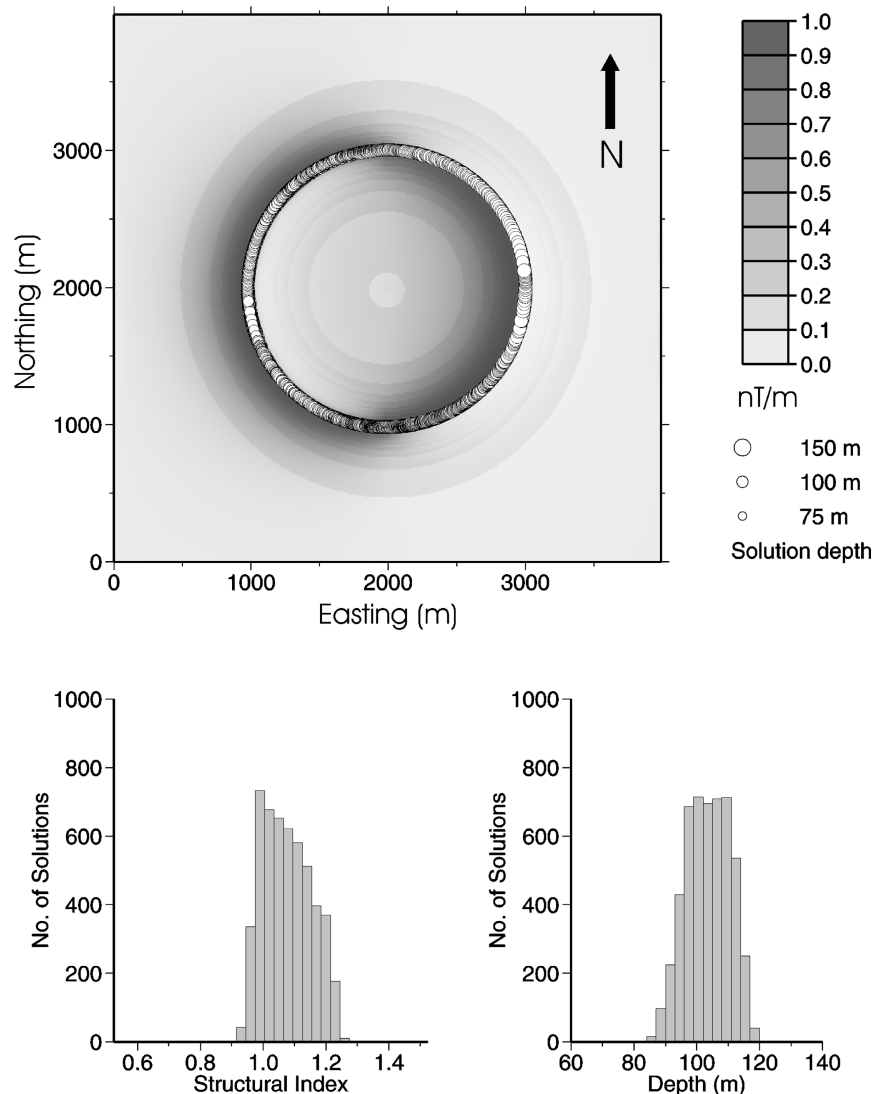


Figure 1 Results of Euler deconvolution of the analytic signal calculated for a thin-sheet model. Top: calculated analytic signal on a 10 m grid. Bottom: histograms of calculated structural index and depth. The model structural index is 2 and the depth is 100 m.

Figure 2 Results of Euler deconvolution of the analytic signal calculated for a vertical cylinder model. Top: calculated analytic signal on a 10 m grid. Bottom: histograms of calculated structural index and depth. The model structural index is 1 and the depth is 100 m.



curvature of the cylinder. Nevertheless, the average depth and structural index are close to their true values. Since most geological structures have some amount of curvature, it can be expected that for gridded data results will not be as good as for profile data.

High-resolution magnetic data are acquired along flight lines spaced typically at 100 or 200 m with a data sampling interval of about 10 m. Data are subsequently interpolated on a grid with an interval equal to about one-quarter of the line spacing. This anisotropy in the sampling interval can lead to interpretation problems, as there is no way to recover the lack of information between flight lines. To simulate this situation, the previous example for the vertical cylinder was resampled at 10 m intervals in the north-south direction and 50 m inter-

vals in the east-west direction. This data set was then gridded at 10 m intervals. The analytic signal structural indices and depths were then calculated. Solutions and their histograms are shown in Fig. 3. These histograms indicate that for this interpolated data set, the analytic signal structural index and depth are both underestimated and that dispersion of the solutions increases. Interpolation increases the high-frequency content in the cross-line direction. This effect is minimal for the total field, but becomes significant for the analytic signal which uses derivatives of the total magnetic field. Computing derivatives is a high-pass filtering operation and, as such, amplifies any noise present in the data. This effectively introduces short-wavelength low-amplitude anomalies in the cross-line direction, resulting in shallower interpreted sources. Their

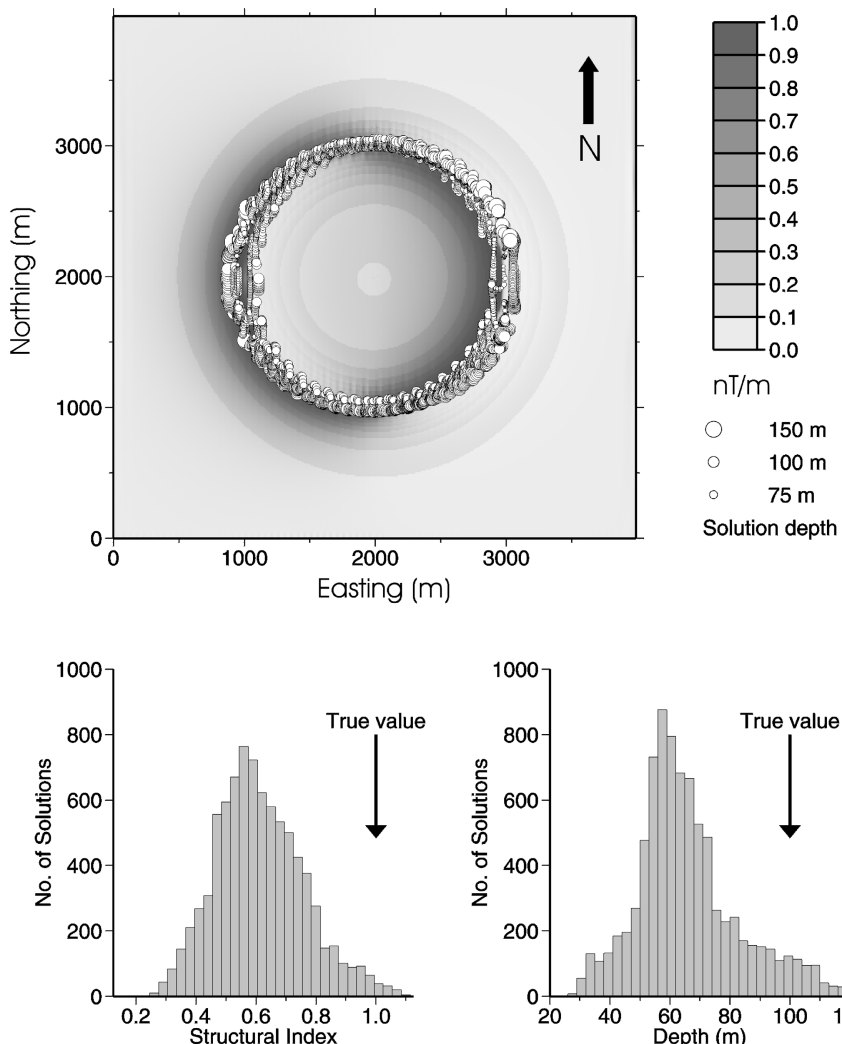


Figure 3 Results of Euler deconvolution of the analytic signal calculated for a vertical cylinder model. Top: interpolated analytic signal on a 50 m grid from data at 10 m spacing N–S and 200 m spacing E–W. Bottom: histograms of calculated structural index and depth. The model structural index is 1 and the depth is 100 m. Interpolation leads to underestimates of both quantities.

exact wavelength is a function of the actual line spacing. An increase in the interpolation noise level results in an increase in solution dispersion.

Another model of interest is the thick dike, as it corresponds to many realistic geological cases such as diabase dikes commonly found in the Canadian Shield or subvertically dipping lava flows. Although the thick dike equation is not homogeneous, it can be expected that a thin dike will be approximated by a thin sheet and a very thick dike by two contacts. The analytic signal structural index is therefore expected to vary between 1 and 2. Tests were made to determine the range of thicknesses where these assumptions are valid. Figure 4 shows the calculated structural index as a function of the thickness-to-depth ratio. Solutions were calculated for a range of spans (5–50 points) and solutions were grouped according to their structural index. Correct structural indices are recovered for

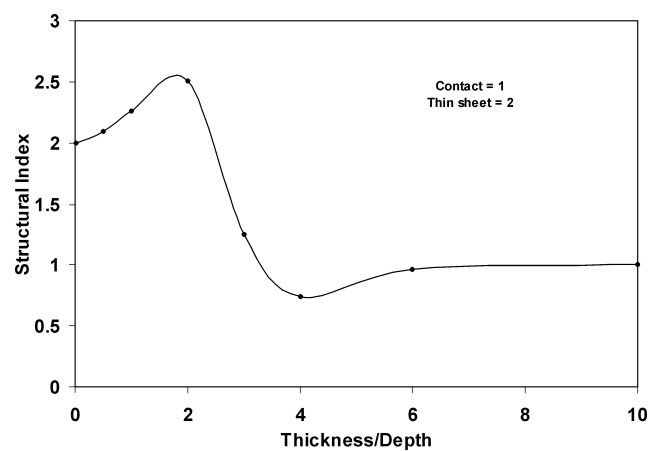


Figure 4 Estimated structural index as a function of the thickness-to-depth ratio for the thick dike analytic signal model.

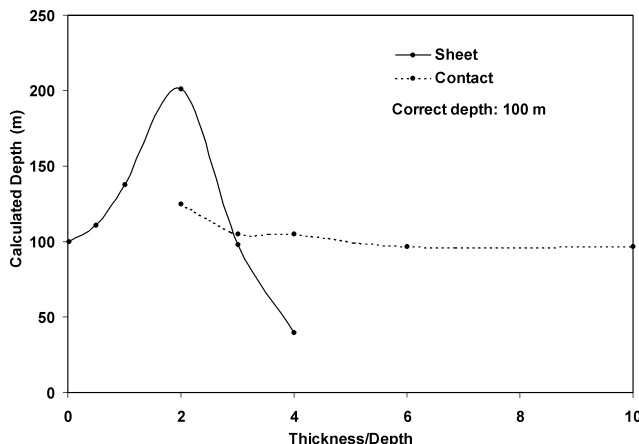


Figure 5 Estimated depths from contact and thin-sheet models as a function of the thickness-to-depth ratio for the analytic signal produced by a thick dike.

thickness-to-depth ratios less than 1 and larger than 5. Depths associated with contact solutions are accurate to better than 5% for thickness-to-depth ratios larger than 3 (Fig. 5), while depths associated with thin-sheet solutions are erroneous by more than 50%. In practice this means that a 50 m-thick dike will be detected as a sheet at a survey height of 100 m, but a 150 m-thick dike will not be correctly identified at the same survey height.

From these theoretical results, it can be expected that the method will perform better for profile data than for gridded data. It is expected, however, to fail for sources of limited lateral extension or with irregular edges and for thick dikes that have a thickness-to-depth ratio between 1 and 5. For profile data, the method will fail for sources of limited lateral extension, as the 2D approximation will be invalid.

CASE HISTORY

Geology

The method was tested on profile and gridded data from an area located in northeastern Ontario, Canada. The region occurs within the Abitibi subprovince which has a general east–west strike and includes many elongated volcanic bands and large granitic intrusions. It is well known for its mineral potential and has been extensively explored. Drill-hole data (Ontario Geological Survey 1999) are available and can be used to determine depth to bedrock in some areas. Drill-hole locations are shown in Fig. 6 and the geology is presented in Fig. 7. Although over 1000 boreholes are available, they tend to be concentrated along specific geological horizons such as the Porcupine-Destor fault zone. Much of the region is covered

by glacial drift and in some areas outcrops are very scarce. Overburden thickness averages 35 m (Jensen, Baker and Trowell 1985) and can be in excess of 50 m, thereby rendering geological mapping very difficult.

The area is cross-cut by two major faults: the Duparquet-Destor-Porcupine break and the Pipestone fault, both generally orientated east–west. Gold deposits are associated with both faults. Rocks of the Porcupine group are located between these two faults and consist of wacke argillite and some carbonate-rich sediments. Rocks of the Stoughton-Rocquemaure group (ultramafic to basaltic-komatiite lavas and Mg-rich tholeiitic basalt) are found to the north and south of the faults. Some ultramafic to mafic sills and stocks also cut the Porcupine group. A few isolated east–west trending dia-base dikes along with a portion of the north–south-orientated Matachewan dike swarm cross the region (Fig. 6).

Geophysical data

Geophysical data were obtained from a combined magnetic-electromagnetic survey flown at a 200 m line spacing in a N30°W direction, perpendicular to the main geological strike of the area (Ontario Geological Survey 2000). The magnetic sensor was located in a bird about 19 m below and 41 m behind the centre of the aircraft. The nominal flight height was 91 m at a speed of 60 m/s. The sampling interval along the flight lines was 12 m on average. Differential GPS was used for flight-path recovery, and laser and radar altimeters were used to determine the height above ground. Magnetic data were gridded at a 40 m interval (Fig. 6). The horizontal derivatives used to compute the analytic signal were calculated in the space domain using a three-point finite-difference operator and the vertical gradient was calculated in the frequency domain. No low-pass filtering was used for the latter.

Flight-line data results

In general there is a good agreement between depths derived from flight-line data and depths from boreholes. However, flight lines rarely pass exactly over a borehole and bedrock topography may vary significantly (Pullan *et al.* 1987; Palacky, Mwenifumbo and Stephens 1992) over a given magnetic anomaly. Examples for three different structural indices are presented and the case of a thick dike is also investigated. These examples are located in the western part of the area studied as this is where the overburden is thicker.

The first example is from line L-81470, where the magnetic anomaly of interest is centred on fiducial 1334. Profile data

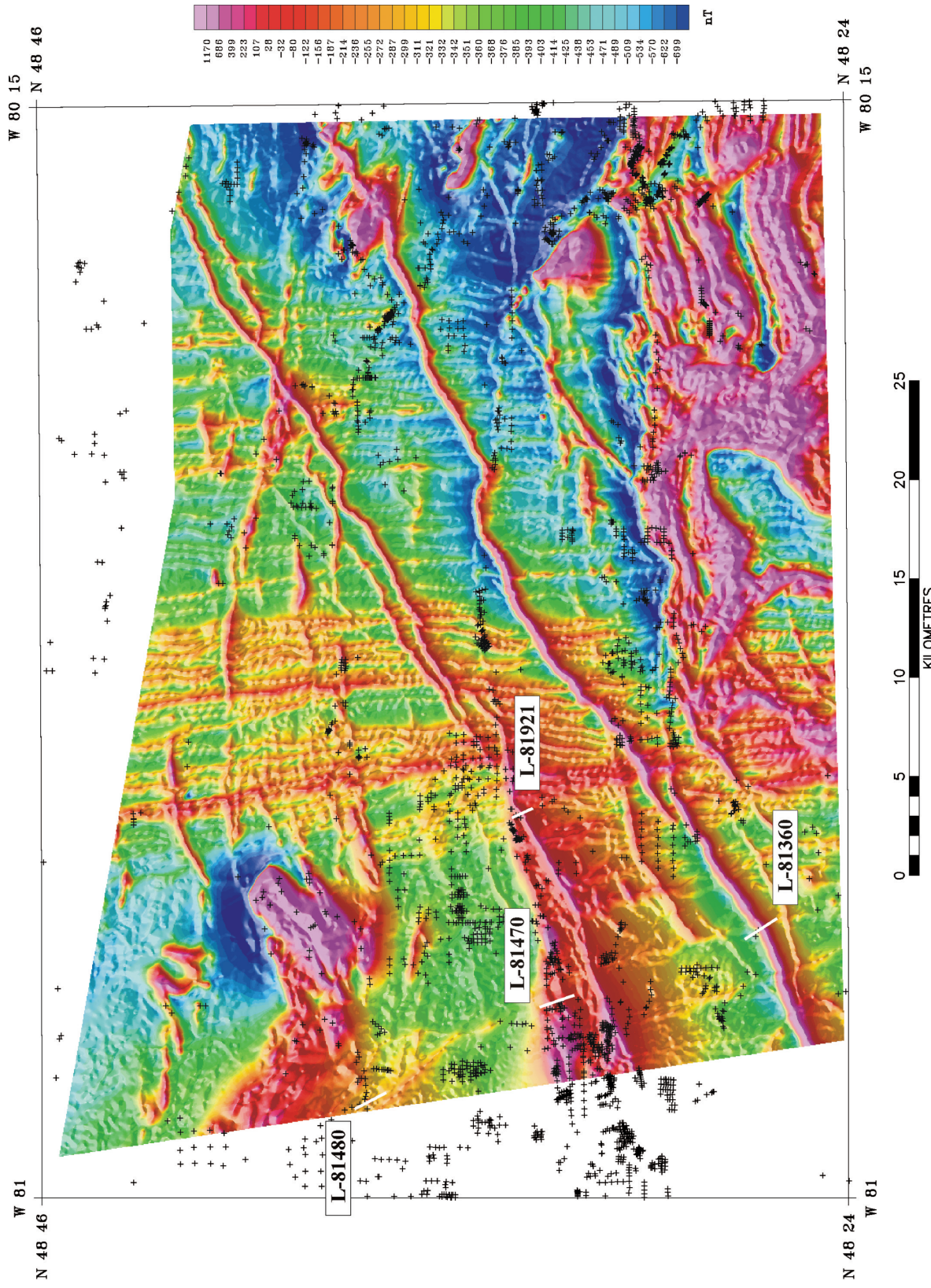


Figure 6 Magnetic field intensity over the Matheson study area, Ontario, Canada. Crosses indicate boreholes from the Ontario Geological Survey database (Ontario Geological Survey 1999). Note the concentration of boreholes along specific horizons.



Figure 7 Simplified geology of the study area. Only major units are annotated. Thick grey lines are diabase dikes, and thick and dotted black lines are mapped and inferred faults. 1: Ultramafic and metavolcanics; 2: mafic metavolcanics; 3: intermediate metavolcanics; 4: felsic metavolcanics; 5: alkalic metavolcanic; 6: alkalic metavolcanic; 7: metasedimentary; 8: clastic metasedimentary; 9: ultramafic intrusive; 10: felsic intrusive; 11: mafic intrusive; 12: porphyry suite; 13: alkalic intrusive. Adapted from Ayer *et al.* (1999).

and deconvolution results are shown in Fig. 8. The interpreted analytic signal structural index is 0.96, which is indicative of a contact, and the interpreted depth is 101 m below the magnetic sensor or 15 m below ground surface. According to the radar altimeter, the magnetic sensor was then 86 m above the ground. The closest drill holes are about 100 m from the magnetic anomaly and their depths vary from 34 to 100 m. From equations (8) and (11), the interpreted dip is 108°. No dip measurements are available, nonetheless this result is in agreement with the fact that the regional geology is known to be subvertical. The depth calculated from (12), assuming an index of 1, is 103 m below the sensor or 17 m below ground surface. The anomaly is located along the Porcupine-Destor fault. Mafic to metavolcanic rocks are on the south side of the fault and clastic metasediments to the north. Ultra-mafic and metavolcanic intrusive rocks are also found along the fault. We interpret the anomaly as being due to the contact between the metavolcanic and the clastic metasedimentary rocks.

The second example is of a thin-sheet anomaly located at fiducial 2182 on line L-81921. The total magnetic field, the analytic signal and the deconvolution results are shown in Fig. 9. The interpreted depth is 139 m below the magnetic sensor or 66 m below the ground surface. The calculated structural index is 2.15, close to the theoretical structural index of 2 for a thin magnetic sheet. The depth calculated from (12), assuming an index of 2, is 132 m below the sensor or 59 m below ground surface. The calculated dip is 104°. The anomaly is clearly associated with a known dike. Although no dip measurements are available, dikes in the area are known to be subvertical. One borehole is located nearby and indicates a depth of 41 m.

A third example is that of a circular anomaly located at fiducial 118 along line L-81480. Profile data and deconvolution results are shown in Fig. 10. Although the anomaly is circular and clearly 3D, use of profile data implies that it is treated as a 2D anomaly. Its average analytic signal structural index is 2.5, close to the theoretical index of a pole, which is 3. Depths obtained from Euler deconvolution are near or at the surface. The depth calculated from (12), assuming an index of 3, is 10 m below ground surface. The nearest borehole is about 200 m to the east and indicates an overburden thickness of 41 m. There is an electromagnetic anomaly associated with the magnetic anomaly and its interpreted depth is 11 m. The anomaly is located along the shore of the Frederick House Lake at the mouth of a small river close to a bridge. Therefore, this anomaly is likely to be cultural in origin.

Finally, we present an example of a thick diabase dike which cross-cuts the southern part of the study area. It has a well-defined magnetic anomaly and an apparent thickness of about 200 m. The selected profile is from line L-81360 and is centred on fiducial 656. The residual magnetic field, its analytic signal and the deconvolution results are shown in Fig. 11. The interpreted depth is 55 m below the surface and a borehole located about 50 m from the line indicates a depth to bedrock of 74 m. The analytic signal maximum is rather flat and has a width of about 150 m. When the relative errors in the structural index computation are plotted as a function of calculated depth or structural index, it can be seen that the smallest errors are associated with the largest depths and structural indices (Fig. 12). This dike was modelled by a dike having a thickness of 250 m, located at a depth of 155 m below the magnetic sensor (Fig. 11b). A susceptibility of 0.0065 SI was used. There is a very good agreement between the calculated curve and the measured data. For perfect data, the number of points used for the deconvolution does not influence the results. It does, however, have some influence on real data. Larger depths tend to be associated with a greater number of points, but the correlation is rather weak (0.31 in this example).

Gridded data results

Solutions from Euler deconvolution of the analytic signal of the magnetic field are presented in Fig. 13. The flight height varies from 59 to 173 m with the average being 96 m. The minimum height of the magnetic sensor was 40 m above ground. Windows of 5×5 and 10×10 data points were used, and solutions with an index of less than 0.5 and a depth to source of less than 40 m were rejected. To check the technique for gridded data, we simply inspected the solutions obtained in the areas previously discussed for profile data.

For the contact example, there are 27 solutions located within 50 m of the average profile solution (L-81470). Their depths vary from 43 to 85 m below the magnetic sensor with an average of 71 m. The average height of the magnetic sensor was 86 m above ground. The analytic signal structural index varies from 0.69 to 1 and the average value is 0.9. The interpreted structural index is very close to the theoretical value, but depths are underestimated by about 50 m.

For the thin-sheet case (L-81921), there are five solutions located within 50 m of the profile average solution. Calculated depths below the magnetic sensor vary between 44 and 57 m

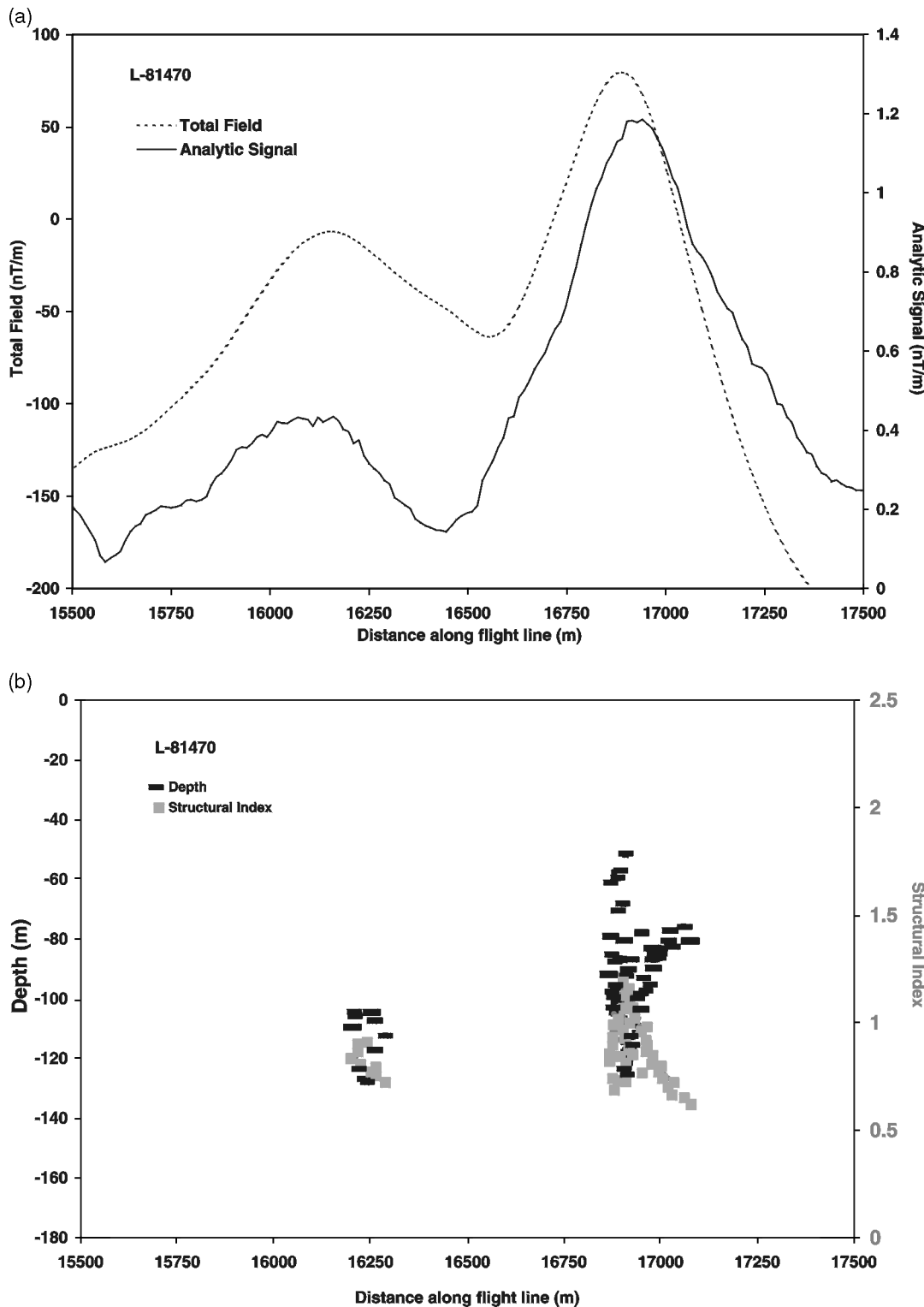


Figure 8 (a) Total magnetic field and analytic signal along a portion of line L-81470. (b) Calculated depths and structural indices from Euler deconvolution of the analytic signal. Solutions discussed in the text are centred at 16 900 m. The average structural index is 0.96, indicating a contact, and the average depth is 101 m under the magnetic sensor.

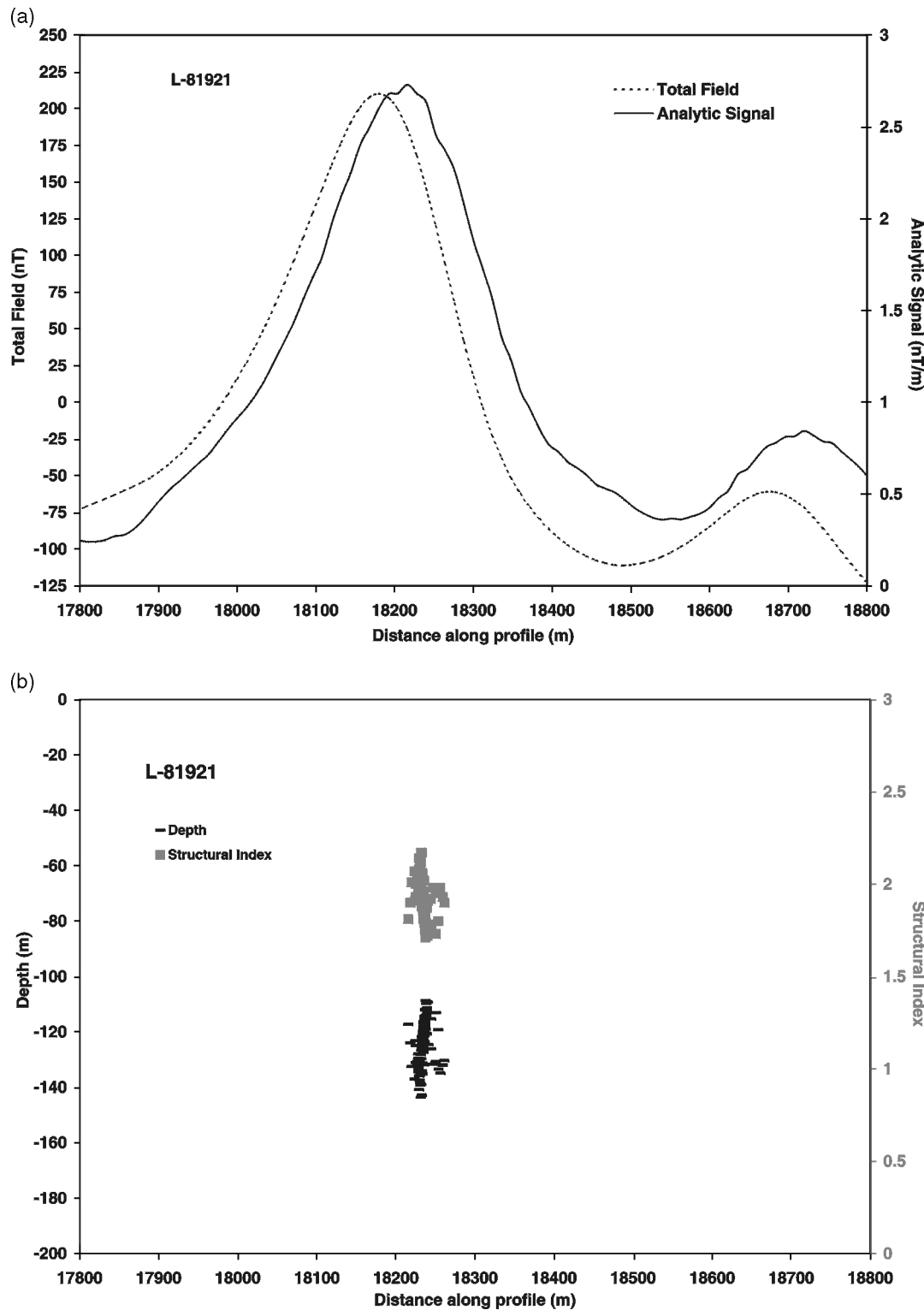


Figure 9 (a) Total magnetic field and analytic signal along a portion of line L-81921. (b) Calculated depths and structural indices from Euler deconvolution of the analytic signal. Solutions are well grouped and show little horizontal dispersion.

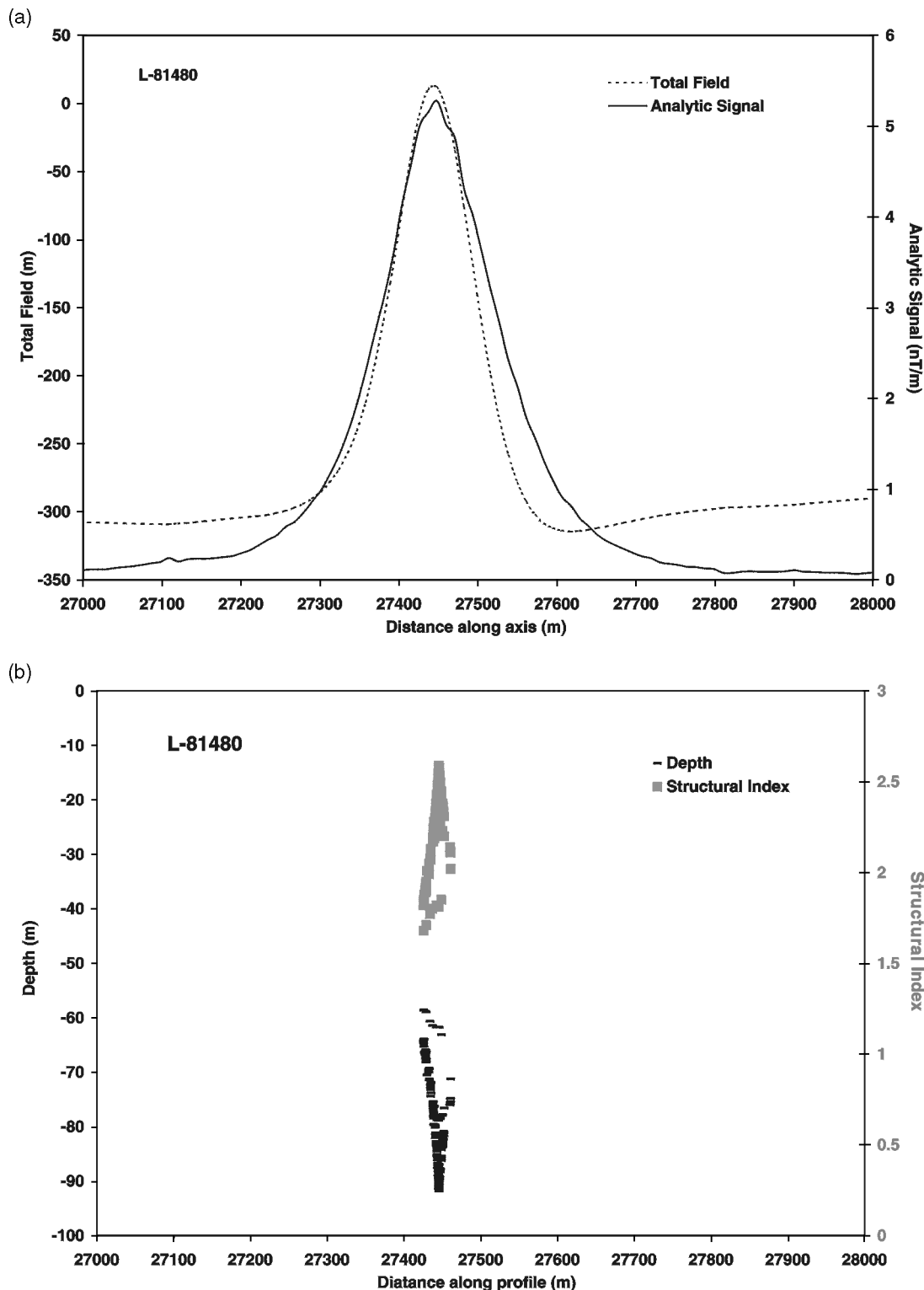


Figure 10 (a) Total magnetic field and analytic signal along a portion of line L-81480. (b) Calculated depths and structural indices from Euler deconvolution of the analytic signal. Solutions show little horizontal dispersion. The structural index peaks at 2.5 and depths vary from 60 to 95 m under the sensor. The high structural index is indicative of a pole.

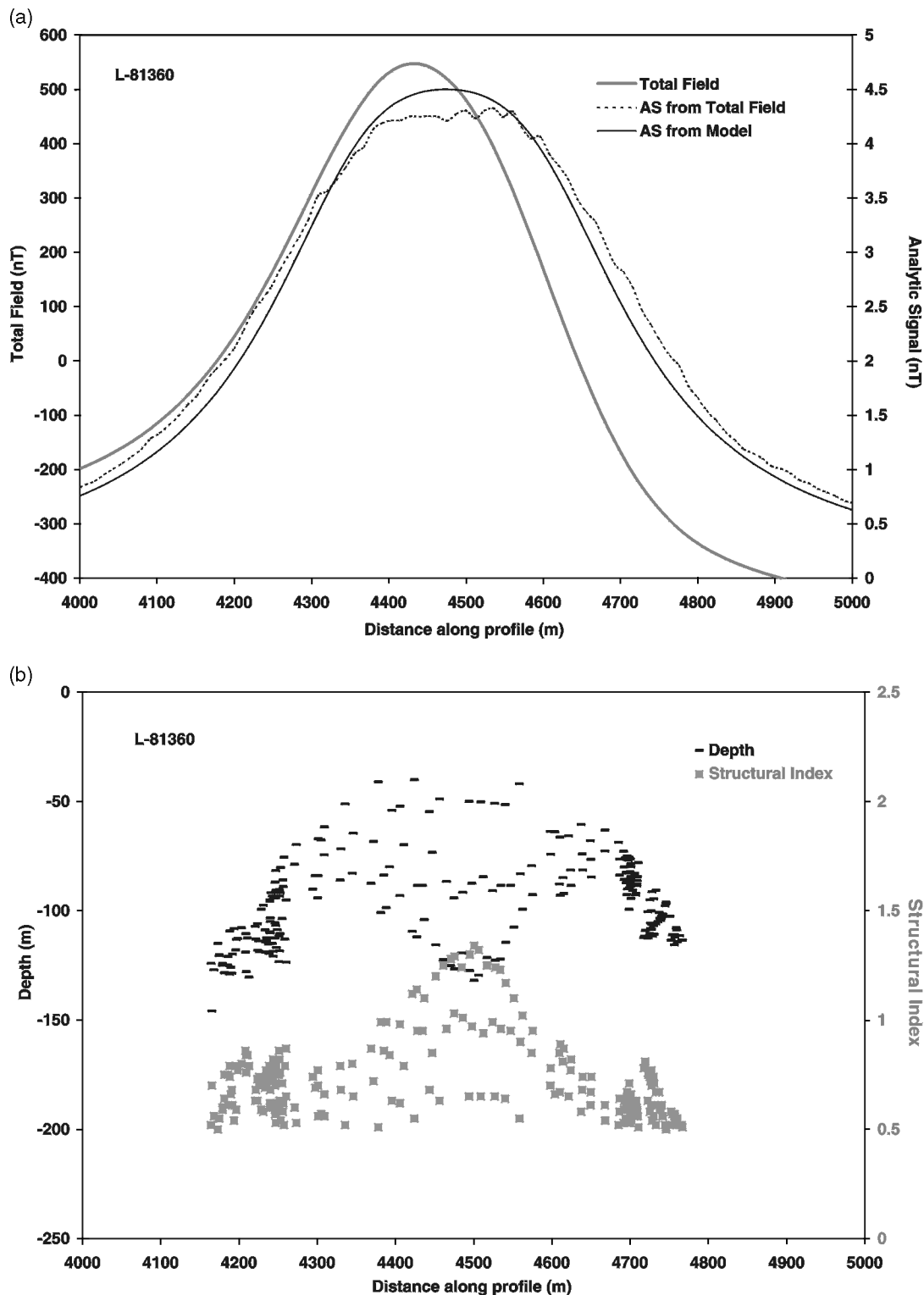


Figure 11 (a) Total magnetic field and analytic signal (from total field observations and from model) along a portion of line L-81360. (b) Calculated depths and structural indices from Euler deconvolution of the analytic signal. Solutions are not well grouped. There are two clusters of solutions located at 4200 m and 4700 m.

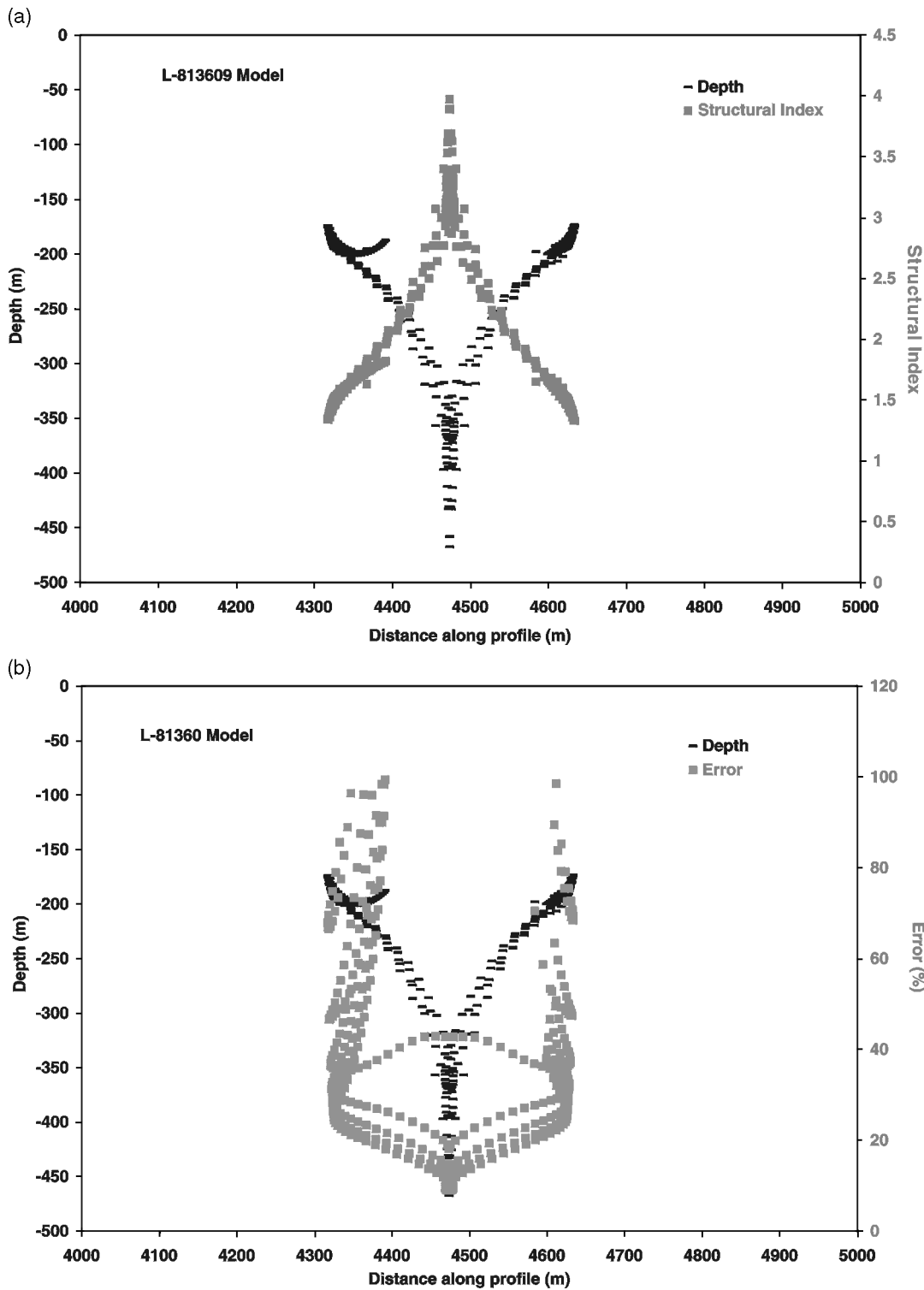


Figure 12 (a) Calculated depths and structural indices from Euler deconvolution of the model analytic signal shown in Fig. 10(a). Note the similarity with the pattern observed in Fig. 11. (b) Calculated depths and percentage errors from Euler deconvolution of the model analytic signal shown in Fig. 11(a). Note that the errors do not show a minimum over the true value of the depth. The minimum error is located over the centre of the dike.

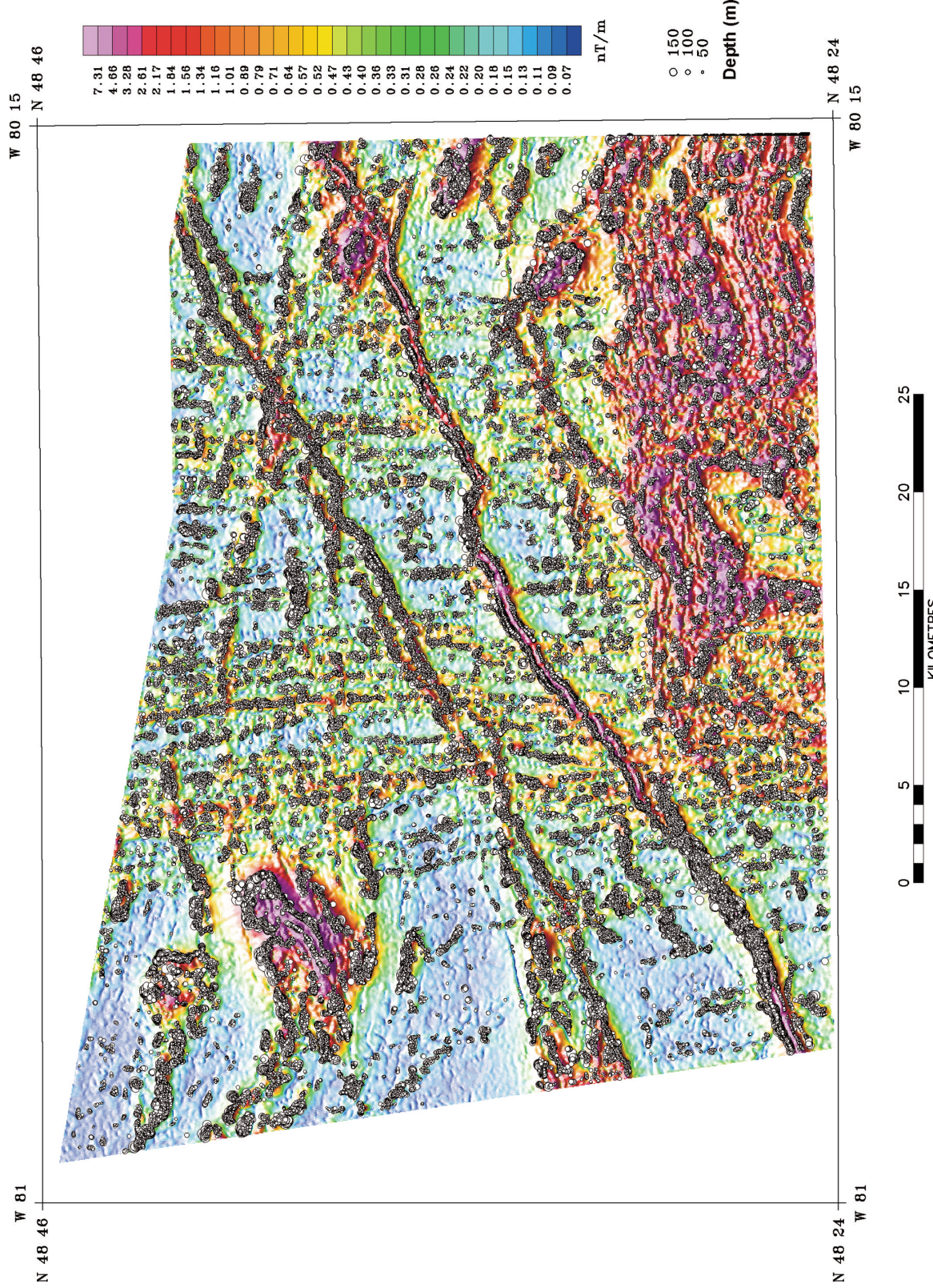


Figure 13 Analytic signal for the Matheson study area, Ontario, Canada. Euler deconvolution results are superimposed with circle size reflecting calculated depths (see legend at right).

and are clearly underestimated as the known depth to bedrock varies from 13 to 41 m and the height of the magnetic sensor above ground was 73 m. The structural index varies from 0.65 to 0.85. In this case, both the depth and the structural index are underestimated relative to the profile results and known values.

For the circular anomaly (L-81480), there are seven solutions located within 50 m of the average profile solution, the analytic signal structural index varies from 1.53 to 1.83 and the depth varies from 43 to 54 m. The structural index is clearly underestimated. If the anomaly is of cultural origin, as suspected, it should be located at ground surface, or about 70 m below the sensor.

For the thick dike (L-81360), two groups of solutions corresponding to profile solutions are located at 4200 m and 4700 m along the flight line. There are six solutions located within 50 m of the 4200 m mark and five solutions within 50 m of the 4700 m mark. For the first group, the average depth is 104 m and for the second group, it is 200 m below the magnetic sensor. This corresponds to depths of 20 m and 120 m below the ground surface as the magnetic sensor was at about 80 m above ground. Two nearby drill holes indicate overburden thicknesses of 74 and 77 m. The analytic signal structural index varies between 0.62 and 0.9 for the first group and 1.1 and 1.2 for the second group. The apparent thickness of the dike is 500 m, much larger than the approximate thickness of 175 m indicated on the geological map.

Clearly, interpolation of data in the direction perpendicular to the flight lines leads to unreliable gradient information. At large distances from the flight lines, the gradients are underestimated since the interpolated field is too smooth. Close to the lines, the gradients are overestimated and lead to underestimates of source depths and structural indices. Such interpolation effects will affect all interpretation methods relying on high-order gradient calculations (e.g. Hsu, Coppens and Shyu 1998; Smith *et al.* 1998).

CONCLUSIONS

Euler deconvolution of the analytic signal of the magnetic field enables the determination of the structural index and source parameters provided that the magnetic field is contaminated only by a constant base level. The results are therefore equivalent to those that would be obtained from deconvolution of the magnetic field in the presence of a constant background field, provided we have *a priori* knowledge of the structural index. Using the analytic signal, it is also possible to determine the dip and the susceptibility contrast. The disadvantage is that

the analytic signal is sensitive to noise in the data and shallow sources are emphasized at the expense of deep sources. Fortunately, the noise level of modern aeromagnetic surveys is very low. The method is also computationally fast and easy to implement.

REFERENCES

- Ayer J.A., Trowell N.F., Berger B., Madon Z., Zalnieriunas R. and Valade L. 1999. *Geological compilation of the Lake Abitibi area, Abitibi Greenstone Belt*. Ontario Geological Survey Miscellaneous Release – Data 46.
- Barbosa V.C.F., Silva J.B.C. and Medeiros W.E. 1999. Stability analysis and improvement of structural index estimation in Euler deconvolution. *Geophysics* **64**, 48–60.
- Hsu S.-K., Coppens D. and Shyu C.-T. 1998. Depth to magnetic source using the generalized analytic signal. *Geophysics* **63**, 1947–1957.
- Huang D., Gubbins D., Clark R.A. and Whaler K.A. 1995. Combined study of Euler's homogeneity equation for gravity and magnetic field. 57th EAGE conference, Glasgow, UK, Extended Abstracts, P144.
- Jensen L.S., Baker C.L. and Trowell N.F. 1985. *Preliminary results of bedrock samples from sonic drilling program in the Matheson area, Cochrane District, Map P. 2848, scale 1:100000*. Ontario Geological Survey.
- MacLeod I.C., Jones K. and Fan Dai T. 1993. 3-D analytic signal in the interpretation of total magnetic field data at low magnetic latitudes. *Exploration Geophysics* **24**, 679–688.
- Marson I. and Klingele E. 1993. Advantages of using the vertical gradient of gravity for 3-D interpretation. *Geophysics* **58**, 1588–1595.
- Nabighian M.N. 1972. The analytic signal of two-dimensional magnetic bodies with polygonal cross-section: its properties and use for automated anomaly interpretation. *Geophysics* **37**, 507–517.
- Ontario Geological Survey 1999. *The Ontario Drill Hole Database. ERLIS data set 13*. Ontario Geological Survey.
- Ontario Geological Survey 2000. *Ontario Airborne Geophysical Surveys, Magnetic and Electromagnetic Data, Matheson Area. Geophysical data set 1101*. Ontario Geological Survey.
- Palacky G.J., Mwenifumbo C.J. and Stephens L.E. 1992. Geophysical studies at the Val Gagné test site, Ontario. In: *Current Research, Part E, Paper 92-1E*, pp. 185–193. Geological Survey of Canada.
- Pullan S.E., Hunter J.A., Gagné R.M. and Good R.L. 1987. Delination of bedrock topography at Val Gagné, Ontario, using seismic reflection techniques. In: *Current Research, Part A, Paper 87-1A*, pp. 905–912. Geological Survey of Canada.
- Ravat D. 1996. Analysis of the Euler method and its applicability in environmental investigations. *Journal of Environmental and Engineering Geophysics* **1**, 229–238.
- Reid A.B. 1995. Euler deconvolution: Past, present and future – A review. 65th SEG meeting, Houston, USA, Expanded Abstracts, 272–273.
- Reid A.B., Alsop J.M., Grander H., Millet A.J. and Somerton I.W. 1990. Magnetic interpretation in three dimensions using Euler deconvolution. *Geophysics* **55**, 80–91.

Roest W., Verhoef J. and Pilkington M. 1992. Magnetic interpretation using the 3-D analytic signal. *Geophysics* **57**, 116–125.

Smith R.S., Thurston J.B., Ting-Fai D. and MacLeod I.N. 1998. iSPITM – the improved source parameter imaging method. *Geophysical Prospecting* **46**, 141–151.

Thompson D.T. 1982. EULDPH – A technique for making computer-assisted depth estimates from magnetic data. *Geophysics* **47**, 31–37.

Thurston J.B. and Smith R.S. 1997. Automatic conversion of magnetic data to depth, dip, and susceptibility contrast using the SPI(TM) method. *Geophysics* **62**, 807–813.